Optimized Design of Opened Quasi-Static Cavity for Omnidirectional Wireless Charging Systems

Cancan Rong, *Senior Member, IEEE*, Qiong Wang, Mengmeng Chen, Yingzhou Guo, Yunpeng Xu, Chenyang Xia, Xian Zhang, and Huamin Jie, *Member, IEEE*

***Abstract*—Optimizing three-dimensional (3D) omnidirectional wireless power transfer (WPT) remains a challenging goal in modern power electronics systems. While several methods, such as orthogonal coil designs and current control strategies have been explored, they still struggle with high degree of freedom charging. Compared to conventional WPT systems, the cavity resonance method offers a promising alternative. This article proposes an opened quasi-static cavity resonance (O-QSCR) structure for this application, which generates a uniform magnetic field throughout the space by driving a wide, even current along its surface. Besides, a method for rapidly evaluating the magnetic field uniformity is introduced to optimize the cavity configuration of O-QSCR based on the magnetic field distribution. Following that, the performance of the proposed O-QSCR system is analyzed using transmission theory and validated through both electromagnetic simulations and experiments. Experimental results show that the transmission efficiency stays above 46% in 95% of the space and exceeds 20% even when the receiver rotates by 60° offset. The proposed system has the capability to light up LEDs at various positions and angles, offering an innovative and practical solution for omnidirectional charging in future 3D environments.**

***Index Terms*—Omnidirectional charging, opened quasi-static cavity resonance (O-QSCR), three-dimensional (3D), wireless power transfer (WPT).**

I. Introduction

WIRELESS power transfer (WPT) technology has been extensively applied in various charging applications owing to its convenience, safety, and effectiveness [1], [2], [3], [4].

Received 23 September 2024; revised 11 December 2024 and 2 February 2025; accepted 18 February 2025. Date of publication 21 February 2025; date of current version 20 March 2025. This work was supported in part by the National Natural Science Foundation of China under Grant 52207019 and Grant 52122701, in part by the State Key Laboratory of Reliability and Intelligence of Electrical Equipment, Hebei University of Technology under Grant EERI_KF2023005, in part by Science and Technology Program of Hebei under Grant 225676163GH, and in part by China Scholarship Council Program (Project ID: 202306420135). Recommended for publication by Associate Editor J. M. Alonso. *(Corresponding author: Cancan Rong.)*

Cancan Rong, Qiong Wang, Mengmeng Chen, Yingzhou Guo, Yunpeng Xu, and Chenyang Xia are with the China University of Mining and Technology, Xuzhou 221116, China (e-mail: ccrong@cumt.edu.cn, elev792@nus.edu.sg; wangqiong@cumt.edu.cn; 17184992@cumt.edu.cn; yzguo@cumt.edu.cn; 09204129@cumt.edu.cn; bluesky198210@163.com).

Xian Zhang is with the Tianjin Key Laboratory of Advanced Electrical Engineering and Energy Technology, Tianjin Polytechnic University, Tianjin 300387, China (e-mail: zhangxian@hebut.edu.cn).

Huamin Jie is with the School of Electrical and Electronic Engineering, Nanyang Technological University, Singapore 639798 (e-mail: jieh0002@e.ntu.edu.sg).

Color versions of one or more figures in this article are available at https://doi.org/10.1109/TPEL.2025.3544237.

Digital Object Identifier 10.1109/TPEL.2025.3544237

For low-power devices (e.g., internet-of-things, swarm robots and household applications), WPT holds great potential for delivering energy cordlessly and effectively [5], [6], [7]. Recent research has increasingly focused on omnidirectional wireless sectors, moving beyond traditional single- or two-direction charging on flat surfaces [8], [9], [10]. A key challenge in this area is minimizing performance degradation caused by either lateral or angular misalignment, making the development of optimized omnidirectional WPT designs crucial.

To date, substantial progress has been established, with two primary strategies to achieve omnidirectional wireless charging: orthogonal coil design and current modulation strategies [11], [12], [13], [14], [15]. Specifically, in [11], a novel quadrature-shaped pickup coil was introduced enabling the angular misalignment-insensitive 3D wireless charging. In [12], a high-efficiency omnidirectional charging system was developed employing an original double toroidal helix coil structure. Similarly, [13] proposed a cubic dipole transmitter coupled with a crossed receiver to maintain stable mutual inductance under the omnidirectional condition. However, these designs often require multiple power sources owing to orthogonal coil configurations, posing challenges in compact applications due to increased complexity and limited range. As an alternative, controling current amplitude and phase angle is effective. In [14], a novel closed-loop-based scheme was proposed to control the magnetic field distribution for high spatial freedom in 2D planar transmitter coil arrays. In [15], nonidentical current control methods were analyzed to generate magnetic fields in all directions for 2D and 3D omnidirectional WPT systems. However, such current regulation techniques rely on external measurement and feedback modules, leading to increased implementation costs.

Metal cavity resonance technology provides useful insights for this field [16]. Traditional cavity resonance enables power transmission by reflecting electromagnetic waves off the metal cavity walls to form a standing wave. In [17], the efficiency of WPT can exceed 60% within around 70% of the wall-meshed cavity area. Nevertheless, the resonant frequency is constrained by the cavity size, typically limited to a few hundred MHz. In addition, the electric field generated inside the cavity could be entangled, which presents a potential safety risk to the human body. To address this issue, the quasi-static cavity resonance (QSCR) was proposed to confine the electric field in the extra central pole [18], [19]. This design effectively isolates the electric field, enhancing safety while ensuring efficient power

TABLE I
DESIGN PARAMETERS FOR THE PROPOSED O-QSCR SYSTEM

Parameter	Description
l/m	Length of the O-QSCR
w/m	Width of the O-QSCR
h/m	Height of the O-QSCR
Al	Metal material of the O-QSCR
t/mm	Thickness of the metal wall
s/m	Length of the coils
$\vec{n}$	Normal vector of the coils

transfer. However, a limitation of QSCR design is the rapid decline in transmission efficiency as the distance from the central pole increases. Additionally, the central pole occupies significant space within the cavity, limiting its practical use. The concept of multimode QSCR was introduced, representing a major advancement in enhancing transmission performance [20], [21]. This approach has two modes, namely pole-independent and pole-dependent in the QSCR, work in conjunction, which can achieve over 37.1% efficiency in the full space. Nevertheless, space utilization within the cavity is still suboptimal due to the central pole's physical presence. Furthermore, the system requires complex control mechanisms and suffers from uneven magnetic field distribution, both of which hinder efficient omnidirectional wireless charging.

Relying on the aforesaid analysis, QSCR provides flexible frequency tuning and enables energy transfer over distances several times the coil size. Its omnidirectional performance is limited due to uneven magnetic field distribution and structural complexity. To overcome these challenges, this article proposes an opened QSCR (O-QSCR) structure for efficient omnidirectional wireless charging. The proposed O-QSCR features a simplified design with significantly enhanced spatial connectivity. By doing so, currents flow uniformly across the metal surface in opposite directions, which creates magnetic field superposition in the cavity's central region. This leads to a more uniform magnetic field throughout the chamber. To optimize the WPT transmission performance, the structural parameters are refined via a tailored magnetic field uniformity evaluation method. The experiment results confirm that the O-QSCR achieves exceptional magnetic field uniformity, making it well-suited for omnidirectional wireless charging.

The rest of this article is organized as follows. Section II describes the characteristics and transmission theory of the O-QSCR WPT system. Section III illustrates the cavity model. Section IV studies the reliability of omnidirectional charging in 3D space via experimental analysis. Section V addresses safety considerations. Finally, Section VI concludes this article.

II. WORKING THEORY AND ANALYTICAL MODELING

A. System Overview

Fig. 1 illustrates a schematic diagram of the O-QSCR WPT system, which primarily consists of a driving coil, a receiving coil, and an opened cavity. A detailed description of the structural parameters is provided in Table I. It is important to note that

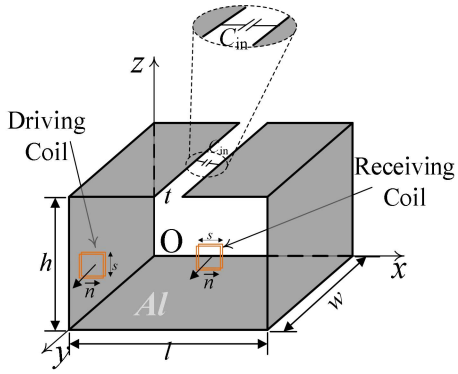

Fig. 1. Schematic diagram of the O-QSCR system used in this article.

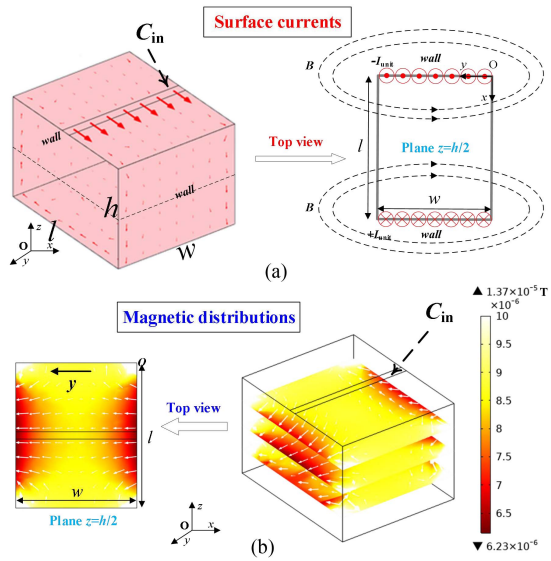

Fig. 2. (a) Surface current distributions of the O-QSCR and the $z = h/2$ plane. (b) Magnetic field distributions of the O-QSCR and the $z = h/2$ plane.

two fully opened surfaces are designed at $y = 0$ and $y = w$. C_{in} is welded at opened joints, which can be used to adjust the working frequency flexibly. The O-QSCR system resonates when the driving coil generates an electromagnetic wave at the same frequency as the O-QSCR. The metal cavity wall acts as a loop for the induced current, generating an effective quasi-static magnetic field throughout the entire cavity. As a result, the receiving coil can be effectively induced when placed at any position inside the cavity.

Indeed, various natural resonance modes arise in the O-QSCR structure due to different surface current distributions. In this article, the primary focus is on the surface current distribution pattern of the cavity current, as shown in Fig. 2(a). In this mode, the surface currents flow along the open section. It can be observed that the direction of the cavity wall currents is opposite at the $z = h/2$ section, and the magnitude is the same, such as $-I_{unit}$ and $+I_{unit}$. According to Ampere's law [22], the magnetic field decreases with distance from the conductor. Additionally, the magnetic fields generated by the surface currents overlap in the central region, causing them to reinforce each other. As a result,

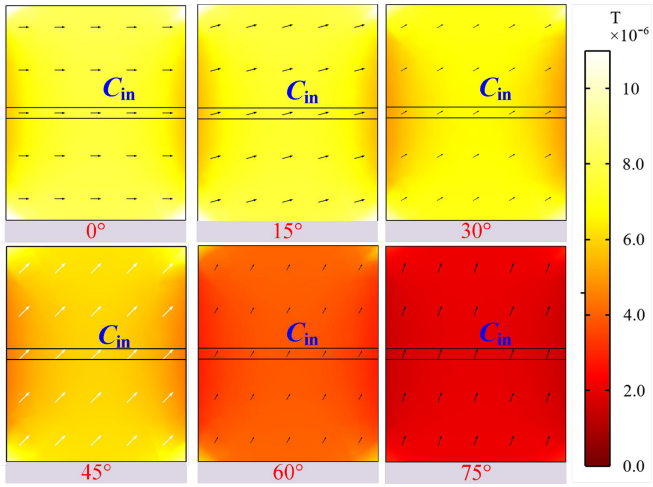

Fig. 3. Magnetic field distributions at various positions and angles within the O-QSCR.

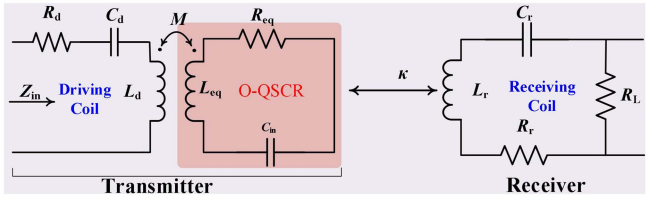

Fig. 4. Schematic diagram of the equivalent circuit for the proposed O-QSCR system.

a uniform magnetic field is established throughout the cavity, as shown in Fig. 2(b). Specifically, the magnetic field directions within the cavity are all perpendicular to the opened plane. This arrangement ultimately enhances the omnidirectional wireless charging performance of the cavity.

The magnetic field distribution at different positions and angles inside the cavity is shown in Fig. 3, where a magnetic field is present in all regions from 0° to 75°. Additionally, it can be obviously seen that the magnetic field of the O-QSCR is uniformly distributed across all directions. Then, the omnidirectional nature of the proposed O-QSCR can be highlighted by the uniformity, and it can enable efficient energy transfer through the magnetic field, except at certain extreme angles.

B. Fundamental of O-QSCR

The magnetic field described above can be generated when the inductive metal wall resonates with the capacitor C_{in}. It is assumed that the inductance of the O-QSCR is L_{eq} and the working frequency is f when the system is in resonance. The finite-element method (FEM) can be used to efficiently and accurately solve for L_{eq}. Additionally, the current distribution can be obtained for different frequencies according to the determined capacitance and structure correspondingly. From this, the unit area current I_{unit} and the total energy α of the magnetic field can be gained accordingly. The relationship among these circuit parameters can be expressed as [20]

$$\alpha = \frac{L_{\text{eq}} I_{\text{unit}}^2}{2}. \tag{1}$$

The resonant frequency of O-QSCR can be tuned by changing C_{in}, which can be derived as

$$C_{\text{in}} = \frac{I_{\text{unit}}^2}{8\pi^2 f^2 \alpha}. \tag{2}$$

The equivalent circuit diagram of the O-QSCR system is shown in Fig. 4. Deriving an effective expression for calculating the mutual inductance between the coil and the metal wall is challenging due to their complex spatial arrangement. Therefore, the FEM is typically employed, in conjunction with coupled-mode theory, to calculate the coupling coefficient [23]. Based on this theory, the coupling coefficient κ can be calculated by the following formulas [16] and [20]

$$\kappa = \frac{\sqrt{2}\omega\beta}{4\sqrt{L_{\text{r}}\alpha}}. \tag{3}$$

Here, L_{r} is the self-inductance of the receiving coil, and β represents the total magnetic flux through the receiving coil. The values of α and β can be determined through the following calculations:

$$\begin{cases} \alpha = \iiint\limits_{V} \frac{\mu_0}{2} \left|\vec{H}\right|^2 dV \\ \beta = \iint\limits_{A} \mu_0 \vec{H} \cdot \vec{n}\, dA \end{cases}. \tag{4}$$

In (4), V is the volume of the O-QSCR, and A is the area of the magnetic flux through the receiving coil. The μ_0 is the permeability of free space. Once the values of α and β have been determined, the coupling coefficient κ can be calculated. Subsequently, the maximum transfer efficiency ($\eta_{\max}$) can be obtained by the following calculations [13], [24]:

$$\eta_{\max} = \frac{\chi\sqrt{1+\chi}}{\left(1+\sqrt{1+\chi}\right)\left(1+\chi+\sqrt{1+\chi}\right)} = \frac{\chi}{\left(1+\sqrt{1+\chi}\right)^2} \tag{5}$$

$$\chi = \frac{4Q_1 Q_2 |\kappa|^2}{\omega_1 \omega_2} \tag{6}$$

where Q_1 and Q_2 are the quality factors of the O-QSCR and the receiving coil, respectively. According to (6), the value of $\eta_{\max}$ at any position of the O-QSCR can be determined by Q_1, Q_2 and the coupling coefficient κ between the two resonators.

III. Model Design and Optimization

As mentioned above, the power transfer efficiency primarily depends on the cavity dimensions and mutual coupling strength. Accordingly, this section is mainly concerned with the optimization of the model design based on the magnetic field uniformity method.

A. Cavity Size Selection

As shown in Fig. 1, the O-QSCR is designed as a rectangle with dimensions $l \times w \times h$ meters for simplicity. The magnetic

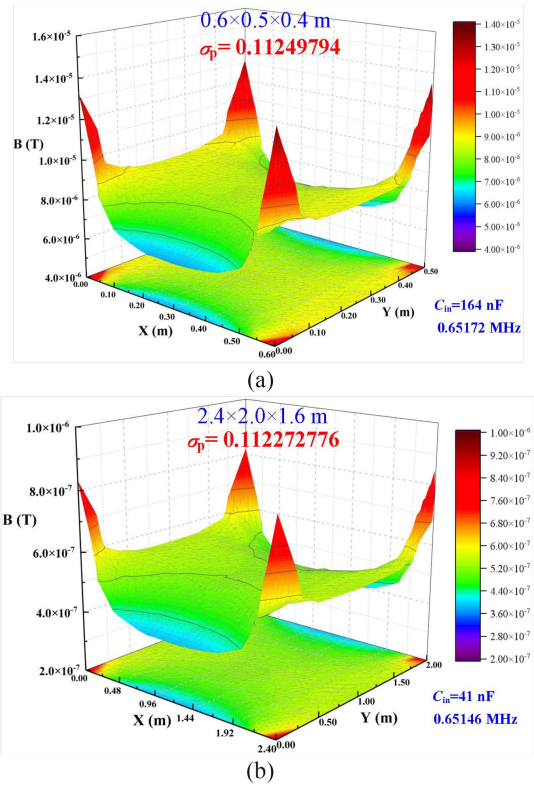

Fig. 5. Magnetic field distribution of O-QSCR and 4 × O-QSCR. (a) O-QSCR. (b) 4 × O-QSCR.

field uniformity within the cavity changes as the dimensions vary. To evaluate this uniformity, the standard deviation method has been developed. In this article, the magnetic field at different cavity dimensions in a specific plane is analyzed to identify the configuration that offers better uniformity. The data from different planes are normalized, as the numerical values of each plane vary. Eventually, the uniformity of the magnetic can be calculated using the standard deviation formula, as follows [25]:

$$\begin{cases} B(i) = \dfrac{B_p(i) - B_{p\min}}{B_{p\max} - B_{p\min}} \\ \sigma_p = \sqrt{\dfrac{1}{n}\sum_{i=1}^{n}\left(B(i) - \overline{B(i)}\right)^2}. \end{cases} \tag{7}$$

In (7), n is the number of selected points for the plane data. Generally, the larger n is, the more accurate the calculation will be. In this article, over 3000 points are selected to ensure accuracy. $B_p(i)$ denotes the magnetic field magnitude at point i on the selected plane. $B_{p\max}(i)$ and $B_{p\min}(i)$ are the maximum and minimum values in the plane data, respectively. $B(i)$ is the magnetic field magnitude at point i after normalization. The symbol σ_p represents the magnetic field uniformity of the plane. In fact, a reduction in the value corresponds to an increased uniformity of the magnetic field distribution.

The magnetic field distribution of the O-QSCR and its amplified quadruple model (4 × O-QSCR) are illustrated in Fig. 5. According to (7), the magnetic field uniformity for the two models are 0.1125 and 0.1123, respectively. It can be observed that the uniformity of the magnetic field is essentially the same

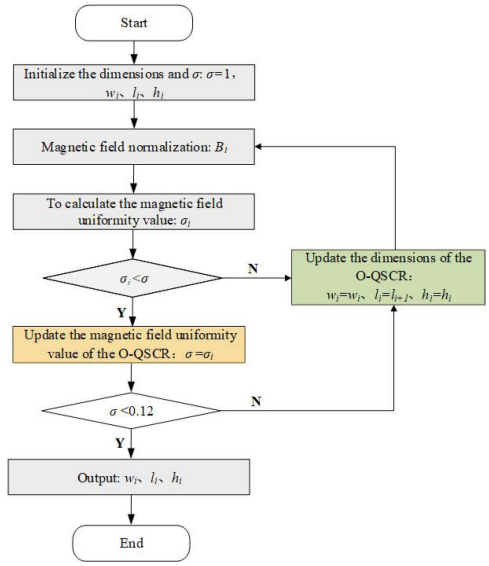

Fig. 6. Flowchart for optimization of cavity dimensions (with the example of optimizing the length l).

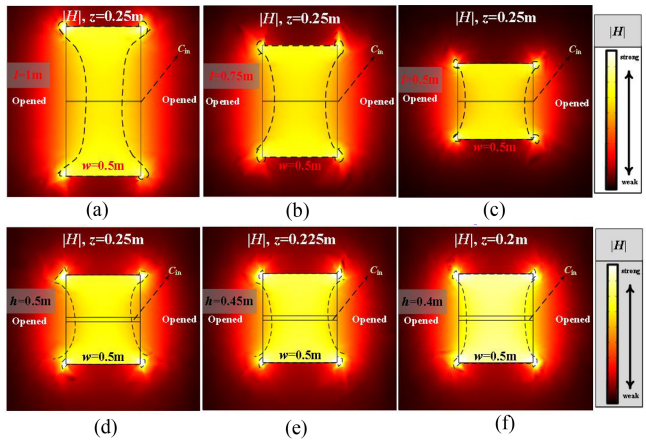

Fig. 7. Magnetic field distributions under different dimensions. (a), (b), and (c) Distribution diagrams as l changes (z = 0.25 m plane). (d), (e), and (f) Distribution diagrams as h changes ($z = h/2$ plane).

for cavities with the same proportions. Based on this observation, this article proposes a method to optimize the cavity size by varying the dimension ratios. The flowchart of O-QSCR dimensional optimization, based on magnetic field uniformity theory, is shown in Fig. 6. The cavity dimensions and the magnetic field uniformity σ are initialized as l_i, w_i, h_i, and 1 (with σ generally much smaller than 1). If the value of σ persistently exceeds a threshold of 0.12, the w_i and h_i parameters remain unchanged, and only the l_i parameter is adjusted until a satisfactory uniform magnetic field is achieved.

In this article, the initial cavity dimensions $l_1 \times w_1 \times h_1$ are set to 1.0, 0.5, and 0.5 m, respectively. At these initial dimensions, the σ_1 is calculated to be 0.1521, as shown in Fig. 7(a). By gradually optimizing the length l, Fig. 7(b) and (c) shows the magnetic field uniformity values of 0.1390 and 0.1180 when l is 0.8 and 0.6 m, respectively. The optimization process that

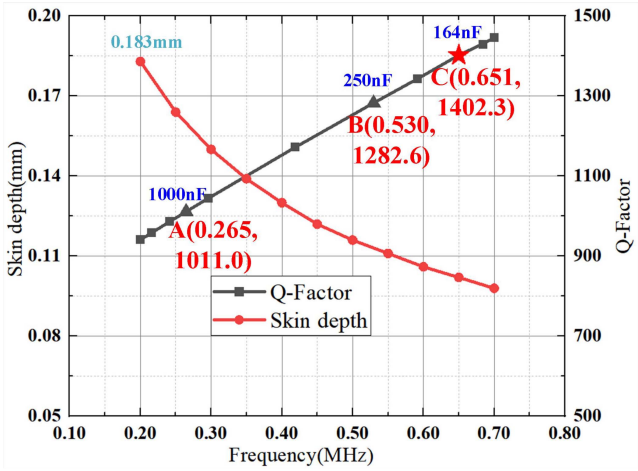

Fig. 8. Relationship between the resonance frequency of O-QSCR and the skin depth and Q-factor, respectively.

reduces the magnetic field uniformity from an initial value of 1 to 0.1180 can be seen as a coarse-grained optimization. Base on the principle, the lower magnetic field uniformity can be preferable, and a fine-grained optimization process (such as adjusting h) is required to further achieve a more uniform magnetic field. During the optimization of h, the values of l and w remain fixed, while h is varied. The results at $h = 0.5$ m, 0.45 m, and 0.4 m can be validated by the FEM simulations, as shown in Fig. 7(d), (e), and (f). It reveals that $h = 0.4$ m can achieve the lowest uniformity value of 0.1125—a 4.7% improvement over the first optimized result. For visual clarity, regions of high field homogeneity are demarcated by dotted-line boundaries, revealing significantly improved uniformity in Fig. 7(f). Consequently, the optimized cavity dimensions are determined to be $0.6 \times 0.5 \times 0.4$ m.

B. System Parameter Setting

Aluminum alloy, chosen for its superior electrical conductivity and efficient heat dissipation properties, is selected as the material for the cavity wall with a thickness of t meters. To ensure effective surface current flow on both sides of the wall and to minimize waste, the thickness is designed to be slightly greater than twice the skin depth (δ). The thickness t can be calculated as [26], [27]

$$\begin{cases} \delta = \frac{1}{\sqrt{\pi f \mu_0 \sigma}} \\ t > 2\delta \end{cases} \tag{8}$$

where the σ denotes the electrical conductivity of aluminum, with a value of 3.774×10^7 S/m.

The thickness of the O-QSCR cavity wall is also dependent on the resonant frequency. As shown in Fig. 8, the relationship between the skin depth δ and frequency is depicted by the red curve. To achieve optimal frequency modulation within a range and to reduce the wastage of metal associated with the selection of excessively thick material, a 0.5 mm thin layer of metal is ultimately selected in this article.

TABLE II
KEY PARAMETERS OF THE WPT SYSTEM

Description	Symbol	Value
Dimension of O-QSCR	$l \times w \times h$	$0.6 \times 0.5 \times 0.4$ m
Quality of the O-QSCR	$Q_{\text{O-QSCR}}$	1402.3
Length of the coils	s	10 cm
Turns of the coils	n	19
Inductance of driving coil	L_{d}	71.10 μH
Inductance of receiving coil	L_{r}	70.97 μH
Quality of the driving coil	Q_{d}	305
Quality of the receiving coil	Q_{r}	312
Working frequency of the system	f	0.651 MHz

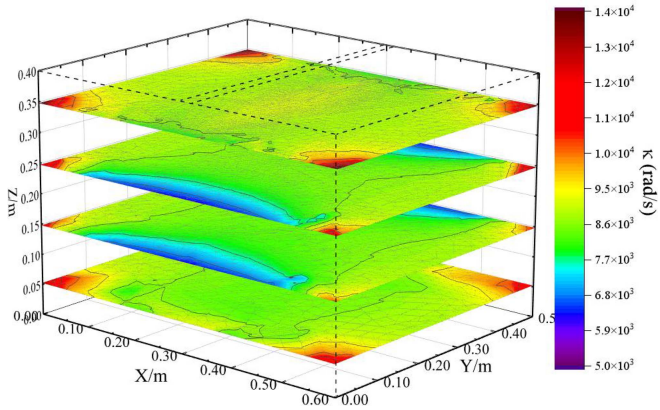

Fig. 9. Coupling coefficients (κ) between O-QSCR and the coils.

According to the finite-element analysis, the simulation results of the quality factor as a function of frequency are represented by gray straight line in Fig. 8. From points A, B, and C, it can be observed that the quality factor of the O-QSCR is proportional to the resonant frequency. As shown in (6), the power transfer efficiency improves as the quality factor (Q) increases. Consequently, the working frequency of 0.651 MHz is selected in consideration of voltage stress caused by higher frequency.

C. Model Efficiency Analysis

Indeed, the size of the coil is primarily matched to the dimension of the cavity in the actual application scenario. To simplify the analytical process, the driving coil and receiving coil are designed as a square spiral coil with 19 turns and a side length of 10 cm in this article. The key parameters are given in Table II. To achieve the better transmission performance, the coupling between the coils and the chamber should be tight. According to (3), the coupling coefficient between O-QSCR and coils in the cavity is calculated as shown in Fig. 9. It is evident that the coupling coefficients are higher at the corners around the O-QSCR, which means the driving coil will have a better effect at these positions.

As illustrated in Fig. 10, the $\eta_{\max}$ at varying heights within the cavity at $z = 0.05$ m, 0.15 m, 0.25 m, and 0.35 m were calculated in accordance with (5) and (6). It can be obviously found that

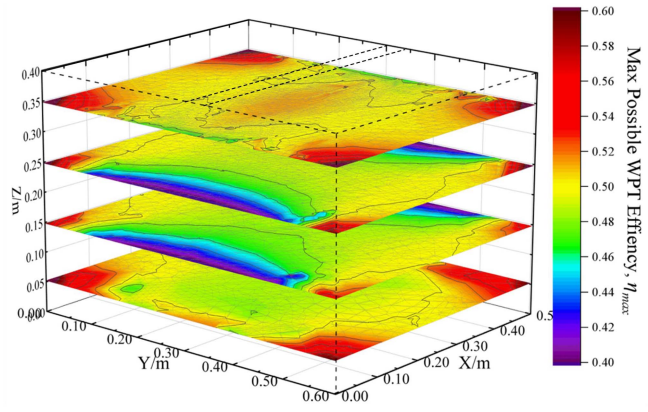

Fig. 10. Maximum transmission efficiency based on coupling with the receiver coil.

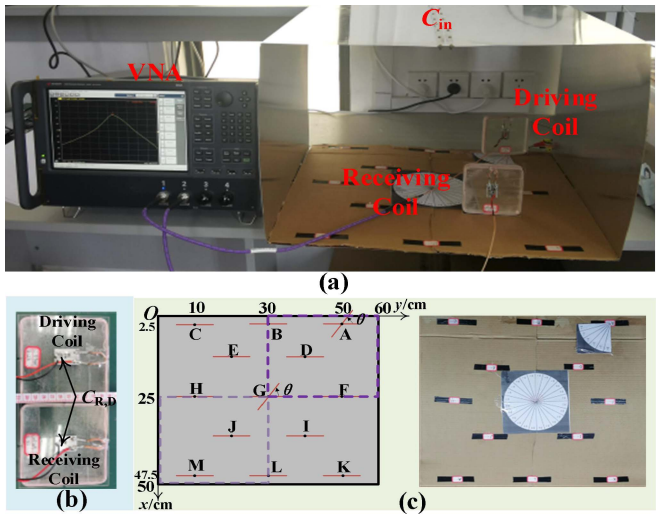

Fig. 11. (a) WPT efficiency of the O-QSCR system based on VNA measurement. (b) Physical diagram of the driving coil and the receiver coil. (c) Cavity is divided into small regions (according to the symmetrically selected purple box, the right panel is the physical diagram).

the WPT efficiencies of most areas maintain between 46% and 52%. Although the WPT efficiency of the opening surface in the middle region and the four corners may fluctuate, it is still within the range of 40% to 60%. Thus, it can be concluded that the transfer efficiency within the entire cavity remains relatively constant. The omnidirectional wireless charging performance is significantly enhanced in the O-QSCR space.

IV. Experimental Verification

In order to verify the omnidirectional wireless charging performance of the proposed O-QSCR, an experimental setup has been established. Initially, the position and angle of the driving coil have been altered with the objective of obtaining the maximum WPT efficiency. Following this, the omnidirectional charging capability across the entire cavity is assessed.

A. Optimal Position and Angle of Driving Coil

As shown in Fig. 11(a), the power transfer efficiency is measured by KEYSIGHT ENA vector network analyzer (VNA) E5080B, and is calculated from the square of the *S*-parameter (S_{21}) [28]. The capacitors are directly connected to the driving and receiving coil for tuning, as illustrated in Fig. 11(b). The key parameters, given in Table II, are identical to those used in the simulation. The selection of design parameters is just for verification of the proposed O-QSCR structure and not intended for optimization of mass, volume and cost.

The gray area in Fig. 11(c) represents the top view of the cavity, which is divided into four parts for measurement. Due to the central symmetry of the cavity structure, the system efficiency at position A is identical to that at positions C, K, M, and others. To confirm that the optimal driving position is at the corners, five representative positions (A, B, D, F, and G) are selected for testing.

As given in Table III, the driving coil is placed at each of these five positions in turn, and the WPT efficiency is measured as the receiving coil is moved from position A to position M. It is important to note that the maximum value in each row is bolded for emphasis. The results clearly show that the O-QSCR

TABLE III
WPT Efficiency at Different Driving Coil Positions

Receiver Position \ Driving Position	A	B	D	F	G
A	-	0.4592	0.4592	0.4624	0.4656
B	**0.4634**	-	0.4550	0.4592	0.4571
C	**0.4786**	0.4508	0.4592	0.4656	0.4592
D	**0.4667**	0.4519	-	0.4467	0.4519
E	**0.4498**	0.4325	0.4335	0.4385	0.4345
F	**0.4613**	0.4446	0.4416	-	0.4426
G	**0.4613**	0.4446	0.4446	0.4436	-
H	**0.4571**	0.4385	0.4406	0.4446	0.4365
I	**0.4677**	0.4508	0.4487	0.4416	0.4467
J	**0.4613**	0.4436	0.4436	0.4467	0.4426
K	**0.4721**	0.4550	0.4571	0.4571	0.4550
L	**0.4677**	0.4487	0.4467	0.4550	0.4365
M	**0.4819**	0.4645	0.4667	0.4699	0.4550

system achieves the highest transfer efficiency when the driving coil is positioned at A. This observation aligns with the results of the coupling coefficient calculations presented in Fig. 10, which are based on the coupled mode theory. Specifically, the coupling coefficient is higher at the corners of the cavity. As a result, the driving coil in the subsequent experiment is placed at A.

The primary loss mechanism in the O-QSCR system is attributed to eddy current losses in the walls. This loss becomes increasingly significant as the angle of the driving coil is rotated. To better understand this effect, the system efficiency was evaluated at various rotational angles of the driving coil. Due to the cavity central symmetry, it suffices to measure the efficiency for coil rotations ranging from 0° to 90° at position A. The VNA is employed to measure the WPT efficiency at discrete angles: 0°; 15°; 30°; 45°; 60°; 75°; and 90°. Subsequently, the system efficiency can be determined, as illustrated in Fig. 12. The results

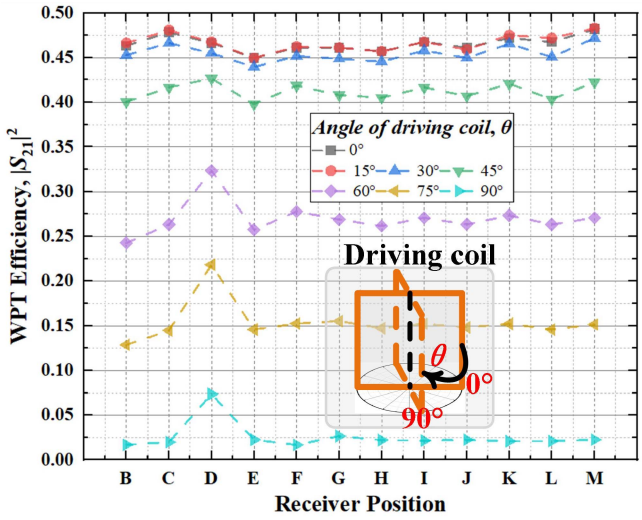

Fig. 12. System efficiency at different driving angles.

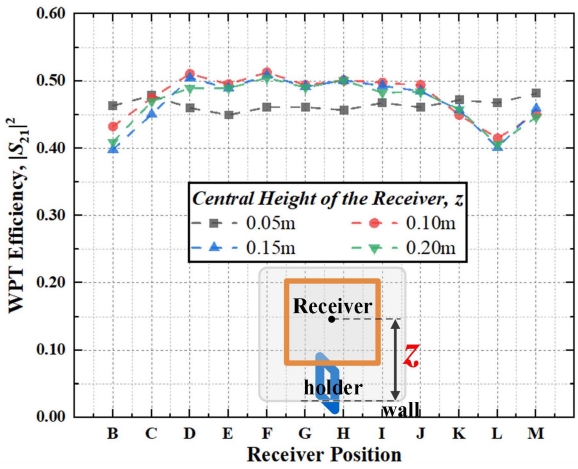

Fig. 13. System efficiency of the receiving coil at different heights.

clearly indicate a decrease in efficiency as the angle of the coil increases. The optimal efficiency can be achieved when driving coil is rotated from 0° to 30°. Therefore, a driving coil angle of 0° was ultimately selected as the optimal configuration to maximize system performance.

B. Reliability Analysis of Omnidirectional Charging

The system efficiency was measured at varying heights and positions of the receiving coil, and the results are presented in Fig. 13. It is evident that the WPT efficiency at heights of z = 0.10 m, 0.15 m, and 0.20 m are nearly identical, indicating a uniform magnetic field distribution across these heights within the O-QSCR system. Furthermore, the 95% cavity demonstrates a WPT efficiency ranging from 46% to 52%, which aligns closely with the theoretical values predicted by coupled-mode theory. These results highlight the O-QSCR system's unique advantage in providing efficient omnidirectional wireless charging.

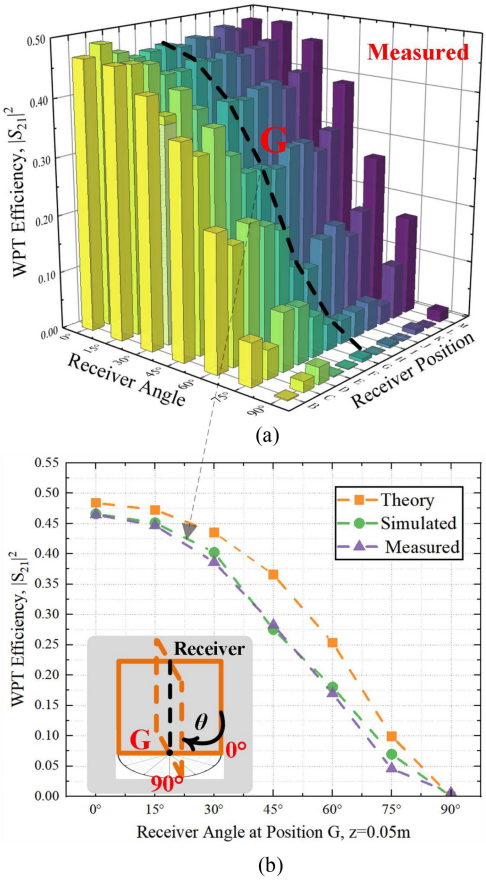

Fig. 14. (a) WPT efficiency of the receiver at different positions and angles. (b) Comparison of calculated, simulated and experimentally measured values.

In order to verify the omnidirectional charging capability in space, the receiving coil is rotated at B-M in the experiments. As illustrated in Fig. 14(a), the WPT efficiency remains relatively consistent across most positions at a given angle, as indicated by the uniform height of the histogram. Furthermore, the trend of these changes with the angle is also consistent, which indicates that the magnetic field is highly uniform in all directions. For a more intuitive representation, Fig. 14(b) illustrates the theoretical, simulated, and experimental measurements as the receiving coil is rotated from 0° to 90° at the representative position. The experimental measurements are highly alignment with the theoretical and simulated values. Additionally, the system efficiency reaches up to 20% in 95% of the cavity areas, even when the coil is rotated to 60°, demonstrating the feasibility of omnidirectional wireless charging.

C. WPT Demonstrations

To intuitively evaluate the feasibility of the proposed system, LEDs were employed as the load for experimental verification, as shown in Fig. 15(a). The LEDs light up when the input voltage exceeds their threshold, with their brightness directly corresponding to the magnitude of the input voltage. This provides further insights into the transmission characteristics of O-QSCR, particularly in terms of omnidirectional performance.

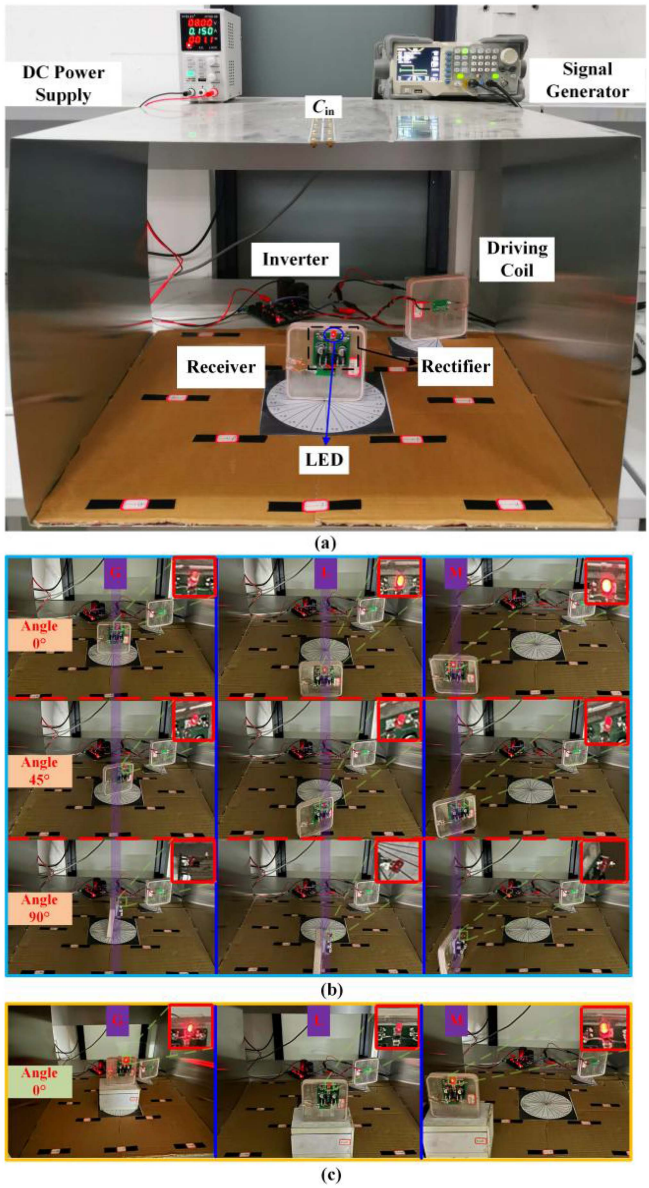

Fig. 15. (a) WPT demonstration based on O-QSCR. (b) Experimental observations of LEDs at different angles (with the center height of the receiver at 0.05 m) for points G, L, M, etc. (c) LEDs experimental observations for points G, L, and M when the center height of the receiver is 0.15 m (with the receiver angle at 0°).

Fig. 15(b) shows the comparative experimental results of the LEDs at different receiving angles, positioned at locations G, L, and M. Through comparing the brightness of these positions at angles of 0°, 45°, and 90°, it can be observed that the LEDs becomes dimmer as the angle increases. Notably, the LEDs do not light up at all when the angle reaches 90°. This phenomenon is consistent with the results shown Fig. 14(b).

Subsequently, the effect of different heights of the receiving coil in the O-QSCR system is also examined. In the experiment, a wooden holder of 10 cm height is placed beneath the receiver coil. The LEDs are lit when the receiver coil is positioned at a height of 0.15 m and an angle of 0°, as shown in Fig. 15(c). It is observed that the brightness of the LEDs decreases at the edges

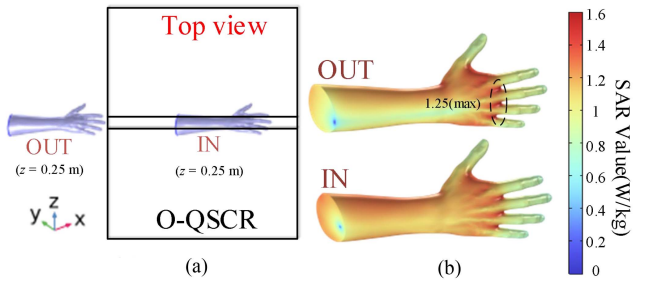

Fig. 16. (a) Top view of the human arm model from the outside into the cavity. (b) SAR simulation results of human arm model under 600 W transmitted power (inside and outside the cavity).

compared to the brightness at a height of 0.05 m, which aligns with the calculated values shown in Fig. 10. Therefore, it can be concluded that the O-QSCR structure can satisfy the normal load operation at any height and any position in 3D space except for some extreme angles.

V. Safety Issue

In daily use scenarios, biological tissues and organs are unavoidably exposed to the magnetic fields generated by the O-QSCR system. To this end, the human arm is employed as a model for simulation analysis in this article. According to IEEE and FCC standards, the specific absorption rate (SAR) of the torso or organism in an exposed magnetic field is usually limited to 1.6 W/kg [18], [29].

As illustrated in Fig. 16(a), a standard SAR analysis is performed by FEM simulations with the model of the human arm developed from the MRI scan. The length of the arm is 0.3 m, which is employed to simulate the scenario when the arm was exposed to the cavity. In order to analyze the safety of the O-QSCR system in both the internal and external space, the labels "OUT" and "IN" are employed to distinguish the spatial state of the arm and the chamber. The SAR values of them scanned are shown in Fig. 16(b). The maximum SAR in the dotted frame at "OUT" reaches 1.25 W/kg as the transmitted port increases its output to 600 W. The SAR value at any position in the cavity is much lower than the limit value. As a result, the O-QSCR system is fully capable of 600 W application scenarios, such as wireless charging cabinets with equivalent power levels. Additionally, the O-QSCR provides a idea for room-level WPT with more uniform magnetic fields in the future.

In terms of tunability, structural complexity, and transmission characteristics, a comparison of O-QSCR with other cavity transmission methods is given in Table IV. Given that the QSCR and M-QSCR methods exist identical polar column, the O-QSCR structure is significantly simple in comparison. The magnetic field uniformity is 0.276, 0.169, and 0.145 when based on CR, QSCR, and M-QSCR transmission techniques with the same dimensions, respectively. A lower value of uniformity indicates a reduction in the degree of magnetic field fluctuation, which signifies a more uniform magnetic field within the chamber. Consequently, the uniformity value of the O-QSCR is 0.110, indicating O-QSCR has a markedly more homogeneous magnetic field than other cavity methods. In conclusion, it can

TABLE IV
COMPARISON WITH OTHER APPROACHES

Ref.	Approaches	Resonant frequency tuning	Structural complexity	Magnetic field uniformity (σ_p)*	Charging area
Kang et al. [16] and Ng et al. [17]	CR	✘ Fixed by cavity dimension	Simple	0.276 (450 MHz)	Eff: over 50% in 95% area
Chabalko and Sample [18] and Yue et al. [19]	QSCR	✔ Adjustable	Complex (Polar column)	0.169 (0.701 MHz)	Eff: over 40% in 80% area
Chabalko et al. [20] and Sasatani et al. [21]	M-QSCR	✔ Adjustable	Complex (Polar column)	0.145 (0.650 MHz)	Eff: over 37.1% in 95% area
This Work	**O-QSCR**	**✔ Adjustable**	**Simple**	**0.112 (0.651 MHz)**	**Eff: over 46% in 95% area**

*: The magnetic field uniformity of different literature methods was evaluated. (The same dimensions as this paper).

be seen that the O-QSCR-based transmission system is more suitable for omnidirectional charging in 3D place.

VI. CONCLUSION

In summary, we propose a novel O-QSCR, providing a simpler and more practical design. The O-QSCR facilitates omnidirectional WPT within a 3D space by effectively distributing surface currents across the cavity. To optimize its design, we propose a method for evaluating the magnetic field uniformity, which aids in determining the optimal cavity size for the O-QSCR model. Subsequently, the WPT efficiency at any position within the cavity can be accurately predicted based on the coupled-mode theory. Experimental results validate these predictions, demonstrating that the transfer efficiency exceeds 46% across 95% of the 3D space, with a cavity volume of $0.6 \times 0.5 \times 0.4$ m. Furthermore, the system retains at least 20% efficiency even with a 60° angular offset, highlighting its robustness. Importantly, the O-QSCR ensures the safety of biological tissues within the charging region, even when operating at an input power of 600 W. Consequently, the O-QSCR offers significant potential for applications in smart homes and intelligent wireless charging cabinets. Future research will focus on increasing the volume and operating frequency to further enhance the system's performance.

REFERENCES

[1] Y. Wang, Z. Sun, Y. Guan, and D. Xu, "Overview of megahertz wireless power transfer," *Proc. IEEE*, vol. 111, no. 5, pp. 528–554, May 2023.

[2] Z. Zhang, H. Pang, A. Georgiadis, and C. Cecati, "Wireless power transfer—An overview," *IEEE Trans. Ind. Electron.*, vol. 66, no. 2, pp. 1044–1058, Feb. 2019.

[3] Q. Wang et al., "Inductive power transfer system with constant current-constant voltage charging tolerating misalignment based on multi-objective optimization for compensation topology," *IEEE Trans. Power Electron.*, vol. 40, no. 3, pp. 4581–4591, Mar. 2025.

[4] C. Rong et al., "Optimization design of resonance coils with high misalignment tolerance for drone wireless charging based on genetic algorithm," *IEEE Trans. Ind. Appl.*, vol. 58, no. 1, pp. 1242–1253, Jan./Feb. 2022.

[5] M. Li and H.-J. Lin, "Design and implementation of smart home control systems based on wireless sensor networks and power line communications," *IEEE Trans. Ind. Electron.*, vol. 62, no. 7, pp. 4430–4442, Jul. 2015.

[6] K. Niotaki et al., "RF energy harvesting and wireless power transfer for energy autonomous wireless devices and RFIDs," *IEEE J. Microw.*, vol. 3, no. 2, pp. 763–782, Apr. 2023.

[7] C. Rong et al., "A comprehensive analysis of metamaterial-coupled WPT systems for low electromagnetic field leakage," *IEEE Trans. Electromagn. Compat.*, vol. 65, no. 1, pp. 166–176, Feb. 2023.

[8] Q. Xu, Q. Hu, H. Wang, Z.-H. Mao, and M. Sun, "Optimal design of planar spiral coil for uniform magnetic field to wirelessly power position-free targets," *IEEE Trans. Magn.*, vol. 57, no. 2, Feb. 2021, Art. no. 4000709.

[9] C. Rong et al., "Optimized design of passive array coils for high efficiency and anti-misalignment WPT system," *IEEE Trans. Power Electron.*, vol. 39, no. 5, pp. 6504–6514, May 2024.

[10] L. Tian, Q. Liu, L. Song, Z. Jin, L. Dong, and Y. Zheng, "Design and optimization of resonance-based wireless power transmission for millimeter-sized planar square inductors micro-magnetic stimulation," *IEEE Trans. Instrum. Meas.*, vol. 72, 2023, Art. no. 4009010, doi: 10.1109/TIM.2023.3292965.

[11] Z. Zhang and B. Zhang, "Angular-misalignment insensitive omnidirectional wireless power transfer," *IEEE Trans. Ind. Electron.*, vol. 67, no. 4, pp. 2755–2764, Apr. 2020.

[12] P. Jayathurathnage, X. Dang, C. R. Simovski, and S. A. Tretyakov, "Self-tuning omnidirectional wireless power transfer using double-toroidal helix coils," *IEEE Trans. Ind. Electron.*, vol. 69, no. 7, pp. 6828–6837, Jul. 2022.

[13] C. Rong, X. He, Y. Zeng, C. Lu, and M. Liu, "High-efficiency orientation insensitive WPT systems using magnetic dipole coil for low-power devices," *IEEE Trans. Power Electron.*, vol. 37, no. 5, pp. 4985–4990, May 2022.

[14] N. Kang, H. Qin, R. Ma, C. H. T. Lee, M. Liu, and C. Ma, "Magnetic field projection and current phase control in a 2D planar transmitting coil array," *IEEE Trans. Power Electron.*, vol. 39, no. 9, pp. 10623–10637, Sep. 2024.

[15] W. M. Ng, C. Zhang, D. Lin, and S. R. Hui, "Two-and three-dimensional omnidirectional wireless power transfer," *IEEE Trans. Power Electron.*, vol. 29, no. 9, pp. 4470–4474, Sep. 2014.

[16] M. J. Chabalko and A. P. Sample, "Resonant cavity mode enabled wireless power transfer," *Appl. Phys. Lett.*, vol. 105, no. 24, 2014, Art. no. 243902.

[17] Z. Yue, Q. Zhang, Z. Yang, R. Bian, D. Zhao, and B.-Z. Wang, "Wall-meshed cavity resonator-based wireless power transfer without blocking wireless communications with outside world," *IEEE Trans. Ind. Electron.*, vol. 69, no. 7, pp. 7481–7490, Jul. 2022.

[18] M. J. Chabalko, M. Shahmohammadi, and A. P. Sample, "Quasistatic cavity resonance for ubiquitous wireless power transfer," *PLoS One*, vol. 12, no. 2, 2017, Art. no. e0169045.

[19] T. Sasatani, C. J. Yang, M. J. Chabalko, Y. Kawahara, and A. P. Sample, "Room-wide wireless charging and load-modulation communication via quasistatic cavity resonance," *Proc. ACM Interactive, Mobile, Wearable Ubiquitous Technol.*, vol. 2, no. 4, pp. 1–23, 2018.

[20] T. Sasatani, A. P. Sample, and Y. Kawahara, "Room-scale magnetoquasistatic wireless power transfer using a cavity-based multimode resonator," *Nature Electron.*, vol. 4, no. 9, pp. 689–697, 2021.

[21] T. Sasatani, M. J. Chabalko, Y. Kawahara, and A. P. Sample, "Multimode quasistatic cavity resonators for wireless power transfer," *IEEE Antennas Wireless Propag. Lett.*, vol. 16, pp. 2746–2749, 2017.

[22] D. K. Cheng, "Fundamentals of engineering electromagnetics," 1993.

[23] H. A. Haus and W. Huang, "Coupled-mode theory," *Proc. IEEE*, vol. 79, no. 10, pp. 1505–1518, Oct. 1991.

[24] M. Zargham and P. G. Gulak, "Maximum achievable efficiency in near-field coupled power-transfer systems," *IEEE Trans. Biomed. Circuits Syst.*, vol. 6, no. 3, pp. 228–245, Jun. 2012.

[25] M. J. Schervish, *Theory of Statistics*. Berlin, Germany: Springer, 2012.

[26] C. Lu et al., "Design and analysis of an omnidirectional dual-band wireless power transfer system," *IEEE Trans. Antennas Propag.*, vol. 69, no. 6, pp. 3493–3502, Jun. 2021.

[27] D. M. Pozar, *Microwave Engineering*. Hoboken, NJ, USA: Wiley, 2011.
[28] C. Rong et al., "A novel equivalent parameter extraction method of cross-frequency metasurface for WPT system," *IEEE Antennas Wireless Propag. Lett.*, vol. 23, no. 11, pp. 3812–3816, Nov. 2024.
[29] A. Christ et al., "Evaluation of wireless resonant power transfer systems with human electromagnetic exposure limits," *IEEE Trans. Electromagn. Compat.*, vol. 55, no. 2, pp. 265–274, Apr. 2013.

Cancan Rong (Senior Member, IEEE) received the Ph.D. degree in electrical engineering from the School of Electrical and Electronic Engineering, Huazhong University of Science and Technology, Wuhan, China, in 2021.

From 2024 to 2025, he was a Visiting Professor with National University of Singapore, Singapore. He is currently an Associate Professor with the China University of Mining and Technology, Xuzhou, China. His research interests include wireless power transfer (WPT) system and metamaterials. He holds 10 patents and authored or coauthored more than 30 papers in prestigious IEEE journals and conferences, such as IEEE TRANSACTION POWER ELECTRONICS and IEEE TRANSACTION INDUSTRIAL ELECTRONICS.

Dr. Rong was the General Co-Chair of IEEE CIYCEE in 2020, Wuhan, China and is General Conference Secretary of ICWPT 2024. He was the Section & Session Chair for numerous international conferences (such as IEEE SPEC, CIEEC, ICEMS, etc.).

Qiong Wang received the B.Eng. degree in electrical engineering and automation in 2021 from Shanghai Maritime University, Shanghai, China. He is currently working toward the M.Eng. degree in electrical engineering with the School of Electrical Engineering, China University of Mining and Technology, Xuzhou, China.

His research focus lies in designing and system modeling of cavity resonant wireless power transfer.

Mengmeng Chen received the B.Eng. degree in electrical engineering and automation in 2022 from China University of Mining and Technology, Xuzhou, China, where he is currently working toward the M.Eng. degree in electrical engineering with the School of Electrical Engineering.

His research interests include the design and modeling of wireless power transfer with relay coils.

Yingzhou Guo received the B.Eng. degree in electrical engineering and automation in 2023 from China University of Mining and Technology, Xuzhou, China, where he is currently working toward the Master of Science degree in electrical engineering.

His research focus lies in designing and system modeling of cavity resonant wireless power transfer.

Yunpeng Xu received the B.Eng. in electrical engineering and automation in 2024 from China University of Mining and Technology, Xuzhou, China, where he is currently working toward the Master of Science degree in electrical engineering.

His research focus lies in designing and system modeling of cavity resonant wireless power transfer.

Chenyang Xia received the B.S., M.S., and Ph.D. degrees in control theory and control engineering from Chongqing University, Chongqing, China, in 2006, 2008, and 2010, respectively.

From 2018 to 2019, he was an Academic Visitor with the University of Auckland, Auckland, New Zealand. He is currently a Professor with the School of Electrical Engineering, China University of Mining and Technology, Xuzhou, China. His current research interests include wireless power transfer and intelligent control.

Xian Zhang received the M.E. and Ph.D. degrees in electrical engineering from the Hebei University of Technology, Tianjin, China, in 2009 and 2012, respectively.

He is currently a Professor with the Hebei University of Technology, Tianjin, China. He is the Director of the China Electrotechnical Society and the Secretary-General of the National Specialized Committee on Wireless Power Transmission Technology. His research interests encompass intelligent high-power wireless power transmission technology, measurement of three-dimensional electromagnetic fields, and numerical calculations of modern engineering electromagnetic fields.

Huamin Jie (Member, IEEE) received the B.Eng. degree in electrical engineering from Wuhan University, China, in 2019, the M.Sc. degree in power engineering, and the Ph.D. degree in electrical engineering from Nanyang Technological University (NTU), Singapore, in 2020 and 2024, respectively.

He is currently a Research Fellow with NTU, Singapore. His research interests include device modeling, electromagnetic interference (EMI), EMI filter design, fault detection, impedance measurement, intentional EMI, and power converter systems.

Dr. Jie was the recipient of the Best Paper Awards at the 2022 Asia-Pacific International Symposium on Electromagnetic Compatibility and the 2023 International Conference on Sensing, Measurement, Communication, and Internet of Things Technologies.